Trueness of digital intraoral impression in reproducing multiple implant position

Short Title: Trueness of intraoral scanners

Ryan Jin-Young Kim[1], Goran I. Benic[2], Ji-Man Park[3*]

[1]Dental Research Institute, School of Dentistry, Seoul National University, Seoul, South Korea.

[2]Clinic of Fixed and Removable Prosthodontics and Dental Material Science, Center for Dental Medicine, University of Zurich, Zurich, Switzerland.

[3]Department of Prosthodontics, Yonsei University, College of Dentistry, Seoul, South Korea.

[*] Corresponding author
E-mail: jimarn@yuhs.ac

Abstract

The aim of this study was to evaluate the trueness of 5 intraoral scanners (IOSs) for digital impression of simulated implant scan bodies in a complete-arch model. A 3D printed full-arch mandible model made of Co-Cr with a total of 6 bilaterally positioned cylinders in the canine, second premolar, and second molar area served as the study model. Digital scans of the model were made with a reference scanner (steroSCAN neo) and 5 IOSs (CEREC Omnicam, CS3600, i500, iTero Element, and TRIOS 3) (n=10). For each IOS's dataset, the XYZ coordinates of the cylinders were obtained from the reference point and the deviations from the reference scanner were calculated using a 3D reverse engineering program (Rapidform). The trueness values were analyzed by Kruskal-Wallis test and Mann-Whitney post hoc test. Direction and amount of deviation differed among cylinder position and among IOSs. Regardless of the IOS type, the cylinders positioned on the left second molar, nearest to the scanning start point, showed the smallest deviation. The deviation generally increased further away from scanning start point towards the right second molar. TRIOS 3 and i500 outperformed the other IOSs for complete-arch digital impression. The accuracy of the CEREC Omnicam, CS3600, and iTero Element were similar on the left side, but they showed more deviations on the right side of the arch when compared to the other IOSs. The accuracy of IOS is still an area that needs to be improved.

Introduction

With the aid of digital technology, traditional dental procedures are continuously being modified and optimized to become more convenient to both patients and clinicians. One of the most significant improvements in digital dentistry is the use of intraoral oral scanners (IOSs) for impression taking. The use of IOSs allows to simplify the workflow for the fabrication of dental restorations by eliminating the rubber-based or alginate impression and preparing stone dies in traditional method, thereby potentially reducing discomfort to patient, introduction of procedural errors and treatment time [1-3].

Since the advent of IOSs, its use has been accepted by many clinicians to adopt digital technology for acquisition of three-dimensional (3D) images of the dento-gingival tissues. For implant placement, IOS enables virtual planning with data from cone-beam computed tomography and fabrication of surgical guides for precise implant positioning. Impression of scan bodies using IOS digitally allows transferring the 3D position of the implant. Although deviation is inevitable during impression taking regardless of the impression technique, impression has to be clinically accurate enough to allow fabricating a well-fitting restoration [4-6]. Misfit of implant-supported reconstructions may not only require more time for clinical adjustment but may also generate stress at the interface between the bone and implant as well as between the implant and prosthetic superstructure. Such stress could in turn potentially cause detrimental biological and technical complications [7,8].

With regard to the accuracy between digital and conventional impression for implant-supported prostheses, controversy continues to exist. Some studies found superior [8,9], some similar [6,10,11], and other inferior [12-17] performance of digital impressions compared to that of conventional impression technique. In these studies, the accuracy of conventional impression was compared to that of digital impressions made by one [6,8-10,12-16] or two

[11,17] types of IOSs. The accuracy of digital impression in partial or complete edentulous model for implant rehabilitation, albeit no consensus, has been compared among IOSs [18-26]. However, there is a lack of up-to-date information as to how various IOSs perform in terms of accuracy in digital implant impression. In addition, recent development of new scanning devices and technology and software upgrade warrants further investigation.

The purpose of this study was to evaluate the spatial accuracy of 5 IOSs in reproducing 6 bilaterally positioned simulated scan bodies in a complete-arch model. The null hypothesis of this study was that that the accuracy of the digital impressions is not different between the IOSs and implant positions.

Materials and Methods

Study model

To replicate a clinical scenario requiring a digital impression of the jaw after placing multiple scan bodies, on a mandibular complete-arch model (E50-500 L; J. Morita Europe GmbH, Dietzenbach, Germany), canines, second premolars, and second molars were trimmed down bilaterally, leaving 1/5 of the cervical portion of the clinical crowns. A digital impression of the model was made with an industrial precision scanner (stereoSCAN neo; AICON 3D Systems GmbH, Braunschweig, Germany). A reverse engineering software (Rapidform; INUS Technology, Seoul, Korea) was used to virtually add a cylinder with a dimeter of 2 mm and height of 7 mm on top of each of the 6 trimmed teeth. Three reference spheres with a diameter of 3.5 mm were added around the left second molar to set the reference three-dimensional coordinate system for the subsequent deviation measurement (Fig 1) [27]. Two spheres were positioned it the lingual aspect; one on the mesial and the other on the distal side of the left

second molar, respectively. Another sphere was located in the distobuccal aspect of the left second molar cylinder to ensure that the coordinates of all the cylinders have positive values.

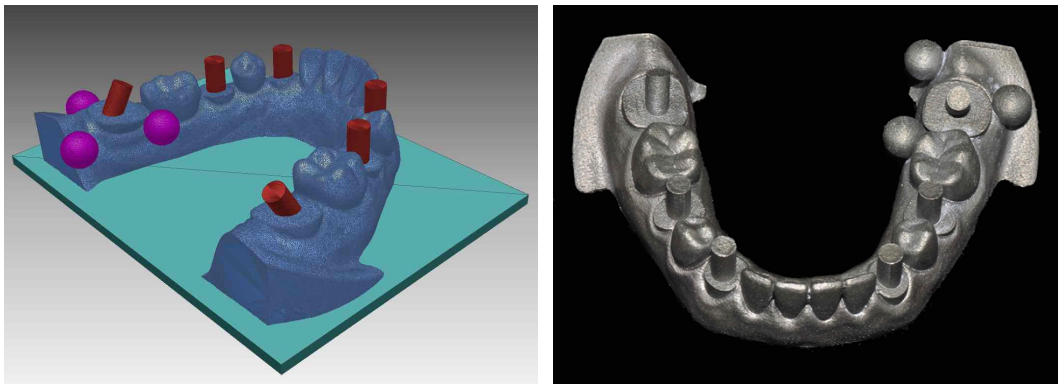

A B

Fig 1. Experimental model. (A) Cylinders and reference spheres digitally formed using a reverse engineering software. (B) 3D printed Co-Cr master model.

The cylinders were positioned perpendicular to the model axial plane, except for two cylinders on the left and right second molars, which were inclined 30 degrees mesially and distally, respectively. A master model made of cobalt-chromium (Co-Cr) was fabricated by a 3D printer (Eosint M270; EOS GmbH, Krailling, Germany) utilizing the direct metal laser sintering technology.

Scanning procedure

The previously described industrial precision scanner was used to scan the 3D printed Co-Cr master model to obtain the reference dataset. Digital impressions of the master model were performed using five IOSs (CEREC Omnicam (Dentsply Sirona, York, PA, USA), CS 3600 (Carestream Health, Rochester, NY, USA), i500 (Medit, Seoul, Korea)), iTero Element (Align Technology, San Jose, CA, USA), and TRIOS 3 (3Shape A/S, Copenhagen, Denmark)) (Table

1). For each scan, the spheres were scanned until no void was observed, and then the scanning procedures for the IOSs were performed along the occlusal surface starting from the left second molar to the right second molar, followed by the lingual and buccal side in the same experimental setting by an operator under ambient fluorescent lighting without the aid of additional lighting. No contrast powder was dusted prior to scanning. Additional scans were made to capture voided area of the cylinders that were critical for measurement. A total of 10 scans were performed by each IOS.

Table 1. Characteristics of intraoral scanners

System	Manufacturer	Scanner technology	Light source	Acquisition method	Necessity of coating
CEREC Omnicam	Sirona Dental Systems	Active triangulation with strip light projection	Light	Video	None
CS3600 i500	Carestream Dental	Active triangulation (Stream projection)	Light	Video	None
iTero Element	Align Technologies	Parallel confocal microscopy	White LED light	Video	None
TRIOS 3	3shape	Confocal microscopy	Light	Video	None

Trueness evaluation of digital impression

The center of the reference sphere in the buccal aspect of the left second molar was set as the origin of the coordinate reference from which deviation of each cylinder was measured in the XYZ axes. The XY plane was formed by connecting the centers of the three spheres. The Y-axis was set as a line parallel to the line connecting the centers of the two spheres in the lingual aspect of the left second molar. The Y-axis denotes the anterior-posterior direction in the XY plane. The X-axis was set as a line perpendicular to the Y-axis, denoting the medial-lateral direction in the XY plane. The Z-axis denotes the coronal-cervical direction from the origin

perpendicular to the XY plane.

The reverse engineering software (Rapidform) was used to obtain the spatial information of the center of the top surface of cylinders in the form of XYZ coordinates from the reference origin for each scan. The coordinate distance between corresponding areas of the reference scan and each intraoral scan was then calculated to obtain the deviations, expressed either in positive or negative value, relative to the reference dataset. For each cylinder position, cumulative deviation in relation to the reference dataset was calculated by the root mean square of the overall XYZ values. The data were analyzed using SPSS Statistics for Windows, Version 23.0 (IBM Corp., Armonk. NY, USA). The Shapiro-Wilk test was carried out to verify the normality of each variable. The median trueness values of the IOSs were analyzed using the Kruskal-Wallis test, followed by Mann-Whitney U test and Bonferroni correction for pairwise comparisons (a =0.05).

For visualization of the distribution of deviation of digital casts obtained by each IOS, an inspection software (Geomagic Verify v4.1.0.0; 3D Systems) was also used to superimpose the 3D digital casts acquired by the reference scanner and each IOS using a best fit algorithm.

Results

The trueness values of the 5 IOSs at each cylinder position in XYZ axes and cumulative XYZ values are presented in Tables 2 and 3. Direction and magnitude of the deviation varied depending on the IOSs and the cylinder location ($P<0.05$). Regardless of the type of IOSs, there was a tendency for the median values and interquartile ranges to increase from the left second molar to the right second molar in the XYZ axes ($P<0.05$) (Fig 2, Table 2). The cumulative XYZ values were not significantly different between the IOSs ($P=0.101$) (Table 3).

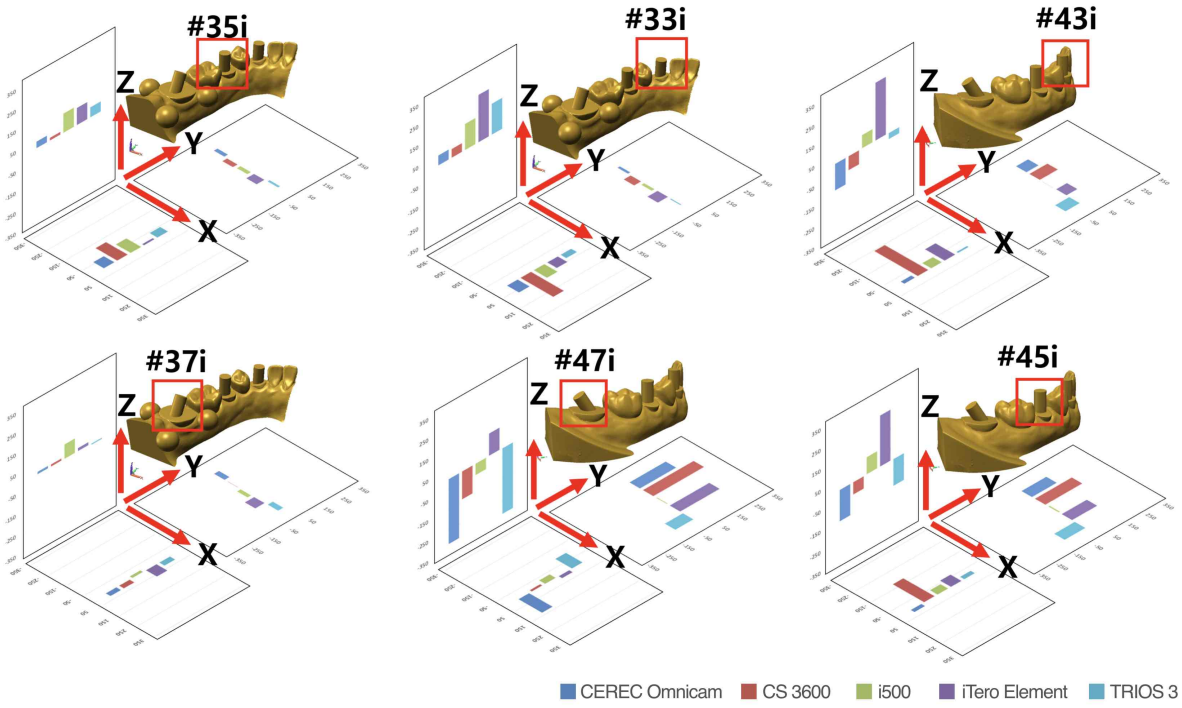

Fig 2. Trueness values (μm) of IOSs at each cylinder position in XYZ axes.

When the root mean square values of the overall XYZ values were pooled together, all the IOSs showed statistically significant gradual increase of the deviation from the left second molar to the right second molar ($P<0.001$) (Table 4). With respect to the overall trueness values, CS3600 showed the highest deviation, while i500 and TRIOS 3 outperformed the other IOSs. On the left side, TRIOS 3 was the only IOS that showed smaller deviation on the left second molar, but no significant difference in the trueness values were found at cylinders positioned on the left second premolar and left canine ($P>0.05$). The trueness values at cylinders positioned on the right side differed significantly among the 5 IOSs ($P<0.05$). The trueness values for CS3600 and CEREC Omnicam were similar to those obtained with iTero Element, i500, and TRIOS 3 on the left side from the second molar to the canine, while their deviation was greater on the right side towards the second molar position (Table 4).

165 Representative color-coded maps of digital casts obtained by each IOS are shown in Figure
166 3. The magnitude and direction of deviations on the color-coded map were not accurately
167 matched with the XYZ deviations of the corresponding areas in Table 2.
168

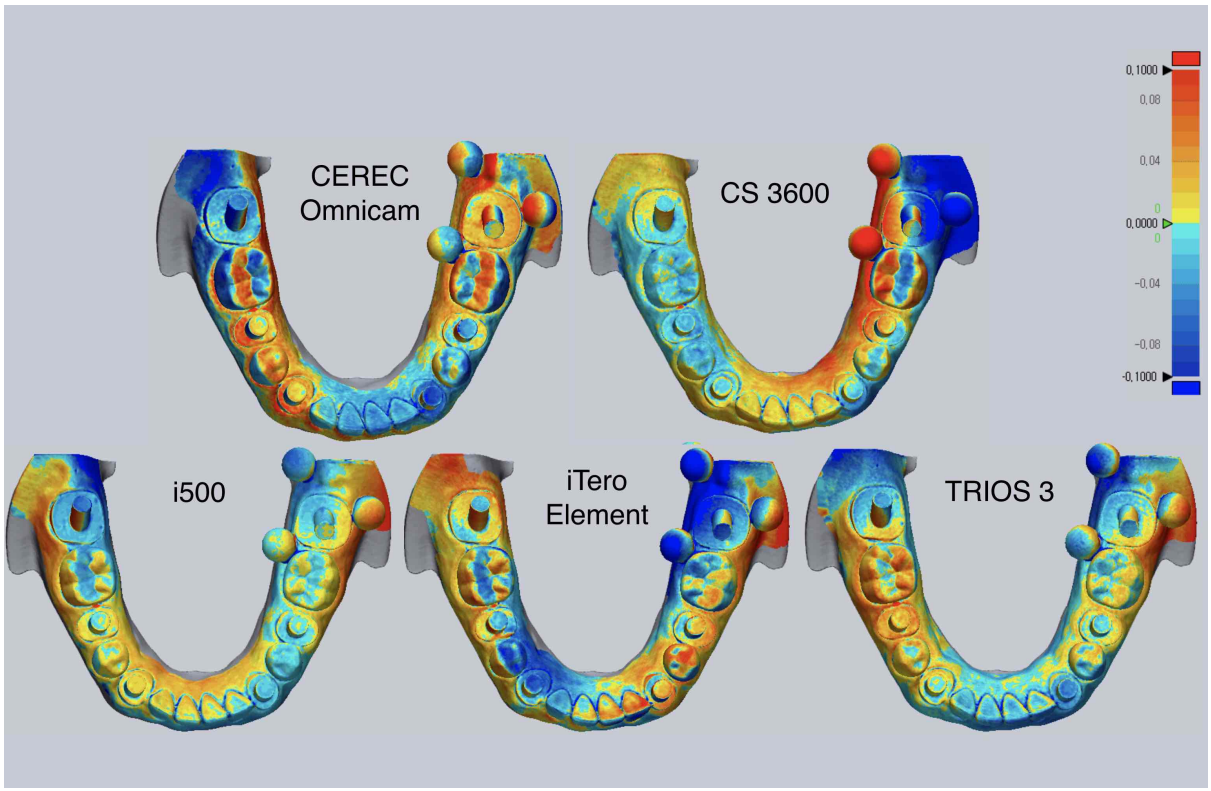

169

170 **Fig 3. Representative deviation of 3D digital casts.** Range of deviation is color-coded from
171 −100 μm (blue) to +100 μm (red).

Table 2. Trueness values (μm) of IOSs at each cylinder position in XYZ axes.

		CEREC Omnicam	CS3600	i500	iTero Element	TRIOS 3	Total	χ^2	df	P
X	37	44.27 [-2.05, 54.64]	29.93 [-4.02, 62.07]	-9.69 [-20.43, -6.31]	60.40 [43.53, 83.24]	28.31 [5.17, 50.38]	**60.38 B [22.45, 96.32]**	16.274	5	0.006
	35	-34.04 [-69.86, 17.08]	-103.48 [169.56, -40.46]	-87.04 [-106.17, -61.91]	-19.64 [-42.76, 11.68]	-38.25 [-95.91, 5.65]	**53.33 B [22.49, 100.51]**			
	33	-24.33 [-96.63, 72.20]	-158.14 [-282.30, -43.58]	-80.111 [-104.85, -53.12]	-78.61 [-106.65, -6.48]	-21.77 [-138.24, 61.29]	**88.01 AB [25.95, 194.09]**			
	43	46.34 [-105.29, 165.76]	-174.68 [-429.17, -122.36]	-61.07 [-77.63, -22.82]	-129.30 [-176.21, -55.59]	3.86 [-122.00, 82.15]	**64.56 AB [30.02, 129.27]**			
	45	64.49 [-23.80, 115.87]	-142.42 [-295.17, -62.95]	-34.02 [-95.24, -4.09]	-81.62 [-103.70, -31.42]	-17.97 [-112.14, 63.33]	**80.88 AB [31.13, 158.88]**			
	47	60.44 [-30.47, 312.78]	29.02 [-153.51, 105.29]	40.66 [-249.60, 137.04]	24.93 [-80.93, 106.14]	-90.37 [-167.36, -23.73]	**105.69 A [59.20, 227.15]**			
	Total	**41.41 b [17.40, 105.36]**	**77.83 ab [40.17, 156.24]**	**88.58 a [51.60, 165.16]**	**64.82 ab [26.42, 124.65]**	**78.41 ab [21.86, 177.00]**	**69.51 [28.86, 142.89]**			
	χ^2	10.147								
	df	4								
	P	0.038								
Y	37	14.12 [-22.11, 44.87]	-12.56 [-28.48, 20.87]	-19.59 [-29.92, -11.64]	-56.55 [-69.82, -24.17]	22.89 [20.34, 33.96]	**65.98 B [40.48, 105.78]**	20.853	5	0.001
	35	11.02 [-28.33, 36.64]	-22.28 [-62.14, 6.25]	-22.32 [-43.29, -6.57]	-42.44 [-67.01, -26.88]	1.17 [-8.60, 39.21]	**59.03 B [18.91, 183.38]**			
	33	-7.38 [-27.98, 46.98]	-42.71 [-83.77, 11.53]	-20.14 [-30.17, 0.86]	-59.03 [-80.04, -45.85]	-3.65 [-36.93, 26.94]	**94.72 AB [29.74, 254.86]**			
	43	17.17 [-145.25, 193.83]	115.47 [-5.02, 181.20]	-21.67 [-77.07, 81.03]	71.05 [15.39, 127.09]	-98.72 [-157.67, 4.16]	**82.61 B [42.69, 174.36]**			
	45	79.83 [-131.15, 310.77]	244.59 [62.40, 289.60]	-11.02 [-88.75, 119.20]	161.01 [58.17, 242.28]	-126.18 [-201.19, -8.47]	**133.91 AB [27.69, 223.38]**			
	47	161.40 [-136.43, 407.79]	279.26 [145.12, 370.96]	-39.42 [-109.46, 142.30]	252.71 [63.21, 352.53]	-98.33 [-218.44, 42.29]	**175.79 A [88.72, 334.19]**			
	Total	**107.62 [51.12, 251.09]**	**81.13 [27.66, 168.70]**	**131.67 [35.49, 282.63]**	**42.45 [22.87, 207.94]**	**95.33 [56.28, 219.53]**	**91.76 [31.96, 218.34]**			
	χ^2	6.537								
	df	4								
	P	0.162								
Z	37	21.39 [-29.31, 31.10]	20.80 [-13.44, 46.13]	67.62 [57.45, 91.50]	30.61 [-29.20, 41.26]	-6.15 [-17.02, -0.94]	**58.21 C [19.00, 110.76]**	40.755	5	<0.001

	35	26.68 [-12.20, 115.37]	48.33 [-41.19, 99.41]	86.05 [61.51, 107.44]	87.21 [34.06, 144.88]	38.44 [12.70, 97.62]	**30.39 C** **[17.52, 77.65]**			
	33	40.03 [-47.37, 191.67]	87.81 [-98.83, 131.79]	119.57 [54.38, 200.77]	205.35 [141.12, 261.26]	117.37 [70.27, 239.92]	**90.45 A** **[54.66, 182.98]**			
	43	-87.47 [-394.93, 82.55]	-162.15 [-343.12, 249.95]	89.63 [-39.50, 223.44]	267.87 [198.11, 369.73]	-67.79 [-86.19, 86.03]	**94.97 AB** **[60.96, 149.63]**			
	45	-131.45 [-359.93, 31.13]	-173.70 [-484.47, 404.43]	60.62 [5.57, 318.74]	244.71 [206.13, 268.88]	-114.11 [-211.72, -48.55]	**66.69 B** **[26.22, 135.08]**			
	47	-257.54 [-437.34, -175.66]	-438.07 [-678.14, 444.85]	-33.51 [-222.06, 165.97]	84.92 [42.15, 220.27]	-314.01 [-439.52, -208.12]	**125.22 A** **[71.31, 288.20]**			
	Total	**77.40 ab** **[30.17, 112.55]**	**67.30 b** **[24.52, 116.74]**	**64.45 b** **[25.32, 123.37]**	**91.59 ab** **[37.10, 174.70]**	**102.32 a** **[51.79, 249.28]**	**76.33** **[31.05, 154.87]**			
	χ^2	13.145								
	df	4								
	P	0.011								

χ^2, chi-square; df, degrees of freedom; P, P-value.
Interquartile ranges [1st quartile, 3rd quartile] are in parentheses.
Positive and negative values indicate deviation to the right and left in X-axis, forwards and backwards in Y-axis, upwards and downwards in Z-axis, respectively.
Absolute values were used for statistical analysis. Different uppercase letters within the same column indicate statistical difference between cylinder positions; different lowercase letters within the same row indicate statistical difference between IOSs (multiple comparison by Mann-Whitney U test with Bonferroni) ($P<0.05$).

Table 3. Cumulative XYZ trueness values (µm) of IOSs.

	CEREC Omnicam	CS3600	i500	iTero Element	TRIOS 3	Total	χ^2	df	P
X	27.10 [-61.05, 87.19]	-90.74 [-185.78, 17.15]	-50.44 [-87.87, -9.14]	-36.65 [-97.75, 56.91]	-13.98 [-103.14, 38.43]	**69.51 B [28.86, 142.89]**	9.347	2	0.009
Y	16.79 [-30.44, 163.25]	23.94 [-28.17, 182.71]	-21.58 [-46.76, 4.26]	-14.38 [-59.67, 144.22]	-10.35 [-107.81, 27.92]	**91.76 A [31.96, 218.34]**			
Z	-7.69 [-203.85, 32.82]	2.65 [-244.74, 97.09]	74.85 [27.40, 149.50]	150.21 [56.97, 257.13]	-15.03 [-117.20, 66.98]	**76.33 AB [31.05, 154.87]**			
Total	**75.07 [25.97, 147.85]**	**72.20 [30.50, 158.58]**	**82.25 [38.20, 171.92]**	**68.52 [26.65, 155.05]**	**90.26 [43.22, 218.02]**	**78.45[30.91, 163.83]**			
χ^2	7.764								
df	4								
P	0.101								

χ^2, chi-square; df, degrees of freedom; P, P-value.
Interquartile ranges [1st quartile, 3rd quartile] are in parentheses.
Positive and negative values indicate deviation to the right and left in X-axis, forwards and backwards in Y-axis, upwards and downwards in Z-axis, respectively.
Absolute values were used for statistical analysis. Different uppercase letters within the same column indicate statistical difference between cylinder positions; different lowercase letters within the same row indicate statistical difference between IOSs (multiple comparison by Mann-Whitney U test with Bonferroni) ($P<0.05$).

Table 4. 3D root mean square deviation (μm) at each cylinder position.

	CEREC Omnicam	CS3600	i500	iTero Element	TRIOS 3	χ^2	df	P	Total	χ^2	df	P
37	75.42 Dab [58.78, 94.39]	55.13 Dab [40.63-95.19]	72.59 Da [58.23, 99.98]	94.52 Ba [69.63, 116.85]	51.40 Cb [41.50, 62.14]	12.240		0.016	**68.07 E [51.90, 94.45]**			
35	123.98 CD [67.77, 157.67]	172.91 CD [94.86-205.98]	121.13 C [108.39, 154.38]	100.21 B [59.63, 161.35]	108.76 C [59.49, 123.96]	5.640		0.228	**116.77 D [74.80, 158.06]**			
33	194.10 BCD [65.53, 273.40]	209.79 BC [156.33-311.33]	144.92 BC [122.79, 217.08]	252.96 A [163.95, 340.71]	171.73 B [136.27, 253.37]	4.950	5	0.293	**187.16 C [145.59, 272.76]**	168.887	5	<0.001
43	289.09 ABCab [211.58, 443.48]	403.42 ABa [194.03-886.19]	204.33 ABCab [129.09, 288.62]	314.61 Aa [267.09, 420.48]	174.98 Bb [166.13, 207.32]	16.794		0.002	**265.51 B [183.49, 401.81]**			
45	498.96 ABa [296.86, 1042.66]	498.96 Aa [296.86-1042.66]	232.14 ABab [146.77, 375.17]	336.04 Aab [272.30, 388.25]	212.64 ABb [156.77, 282.71]	19.517		0.001	**322.01 AB [234.87, 497.31]**			
47	555.83 Aab [292.39, 647.73]	670.89 Aa [472.81-1054.51]	314.71 Ab [230.34, 518.94]	343.99 Ab [168.54, 406.92]	378.94 Ab [259.38, 514.09]	13.416		0.009	**405.96 A [272.98, 585.61]**			
χ^2	32.280	40.788	36.294	38.481	36.867							
df	4											
P	<0.001	<0.001	<0.001	<0.001	<0.001							
Total	**230.93 ab [94.39, 492.62]**	**252.68 a [147.22, 532.77]**	**150.34 b [109.63, 262.59]**	**258.10 ab [117.43, 353.35]**	**165.40 b [75.16, 245.09]**				**195.33 [109.22, 357.99]**			
χ^2	16.885											
df	4											
P	0.002											

χ^2, chi-square; df, degrees of freedom; P, P-value.
Interquartile ranges [1st quartile, 3rd quartile] are in parentheses.
Different uppercase letters within the same column indicate statistical difference between cylinder positions; different lowercase letters within the same row indicate statistical difference between IOSs (multiple comparison by Mann-Whitney U test with Bonferroni) ($P<0.05$).

Discussion

Scan bodies have been used in the digital workflow of implant dentistry to supplant traditional impression procedure by digitally transferring the position of implant, saving cost and time for the clinicians and dental technicians, and reducing patient's discomfort during impression taking [2,3,28]. New IOSs are being developed and have emerged on the market, while existing IOSs are also continuously being upgraded to a newer version of software to enhance their performance. The rising demand in digitalization by both dental team and patients is likely set the use of IOSs as the norm in routine daily practice after a satisfactory level of consensus on the application of IOSs for digital impression is clearly reached.

In this context, the present study was designed to clarify the performance of IOSs by evaluating the accuracy of 5 IOSs for acquisition of digital impressions of 6 simulated scan bodies that were bilaterally positioned in a complete-arch model. To ensure the same testing condition, a commercially available assortment of artificial teeth that were screw-retained to a lower model was scanned, and the master model made of Co-Cr was fabricated by 3D additive manufacturing after modelling the cylinders to simulate screw-retained scan bodies. The dimensionally stable master model eliminated possible errors that could have occurred if external forces had been inadvertently applied to the screw-retained components during the experiment. The present study demonstrated that the accuracy of digital impressions varied significantly by IOSs and cylinder position. Therefore, the null hypothesis of this study that the IOS type and cylinder location would not affect the accuracy of digital impressions was rejected.

With regard to the cylinder position, deviation from true value was smallest at the cylinder located on the left second molar from which complete-arch digital impression was sequentially made to the right second molar. Although some authors claimed that no significant differences

in trueness were found between partially and completely edentulous implant models [22], arch length has been generally considered major culprit behind the development of deviation in a 3D virtual model due to the limited field of view of each capture using IOS. Captured multiple images are combined together by continuous stitching process at overlapping portion of the images, which is known to be the cause of deviation in a digitized model, processed by the proprietary software. This cumulative error accounts for the tendency for longer scanning span to generate greater chance of errors during the image combining process [4,19].

The overall accuracy was found to be best in the i500 and TRIOS 3 (Table 4). They also showed more consistent accuracy than the iTero Element, CEREC Omnicam and CS3600, which were, however, similar to the other IOSs on the left side from the second molar to the canine. In terms of precision, which indicates the degree to which images acquired by repeated scanning are identical, the range of trueness values could be used to deduce the precision of each IOS. The significantly greater range of trueness values were noted particularly in the CEREC Omnicam and CS3600 towards the opposite side of the origin of scanning. Within the limitations of the present study, the marked distortion on the right side suggests that the CEREC Omnicam and CS3600 may be well suited for unilateral partial-arch impression rather than for complete-arch scanning.

In a previous study that compared the accuracy of CEREC Omnicam, CS3600, TRIOS 3, and True Definition, CS3600 was found to be the best performing IOS [21]. The authors evaluated the entire trueness of each IOS for implant impression in a partially or a completely edentulous model using superimposing technique. The difference in the findings between this study and the present investigation might be explained by the different methodology employed for determining trueness. The present study measured the XYZ 3D displacement of the centroid of each cylinder. Thus, the XYZ deviations shown in Table 2 and Figure 2 were not accurately coincided with the corresponding areas on the color-coded map presented in Figure 3. The

color-coded map is generated by superimposing datasets of the test group on to that of the reference scanner. Despite the fact that the color-coded map provides a general visual overview of scanning discrepancy by translating 3D deviation into 2D color-codes, superimposition by arbitrarily programmed best-fit may not be the most appropriate method in determining the trueness of IOSs at a specific location of interest. On the contrary to the previous studies that demonstrated only linear deviation [18-22], the XYZ coordinates used in the present study enabled precise acquisition of 3D spatial information of the individual cylinder by obtaining the differences of corresponding XYZ coordinates between the reference and test groups datasets. Direction and magnitude of the deviation in the XYZ axes varied depending on the IOSs and cylinder location. Insignificant differences in the cumulative XYZ total values among the IOSs (Table 3) was associated with the masking effect that yielded smaller cumulative deviation than the actual deviation due to the positive and negative values within the groups. The root mean square of the overall XYZ values were also calculated to directly compare the actual discrepancy of the digital impressions for each IOS. The findings of the present study were consistent with previous studies on the accuracy of digital implant impression that reported greater distortion with an increase in the scanning length [18-21,24-26].

IOS uses specific principle to acquire digital images of a real object. Although different data capture principles may be associated with the accuracy of IOS, based on the current literature, direct technique is deemed to provide more accurate impression as the number of implants increases [8,29]. But it cannot be asserted that the decrease in accuracy is directly attributable to the number of implants. Inaccurate digital impression in implant rehabilitation directly leads to mispositioning of virtual implant fixture which in turn may cause misfit of a fabricated prosthesis. From the biomechanical perspective, poorly fitting superstructures may be a detrimental factor to the longevity of restorations due to undue stress between the components [7,8].

For making impressions of a multiple angulated implant condition, digital impression could be a preferred approach given deformation of impression material during removal. As the angulation of implants increases, the impression material could be more distorted when removing it from the undercut areas. Nevertheless, the more implants that are being scanned, the longer the length of span that requires a greater number of images, theoretically resulting in a greater degree of cumulative errors. In our study model, accuracy of digital implant impression was evaluated in the dentate model, and this study confirmed that not all IOSs reproduced the same accuracy because of the differences in the data capture mode, principle, or software algorithms used in each IOS. This study also showed that some IOSs require further improvement to attain comparable accuracy. The size of the edentulous region should also be taken into consideration when investigating the accuracy of IOSs, since the lack of anatomic landmarks in smooth-surfaced soft tissue of edentulous region hampers the superimpositions the scans, [30]. Further studies should evaluate the influence of teeth or edentulous span between implant scan bodies to provide a better understanding of the edentulous span on the digital impression accuracy.

Conclusions

Within the limitations of the present study, all the IOSs exhibited increasing deviation with an increasing distance from the start position of scanning. The direction and magnitude of deviation differed among jaw regions and IOSs. All the IOSs were similar for unilateral arch scanning, while i500, and TRIOS 3 outperformed the other IOSs for complete-arch scanning. The accuracy of IOS requires additional improvement.

Acknowledgements

This study was supported by a grant of the Korea Health Technology R&D Project through the Korea Health Industry Development Institute (KHIDI), funded by the Ministry of Health & Welfare (HI18C0435). We thank J. Kim for technical assistance with sample preparation.

Author Contributions

Conceptualization: Ji-Man Park.

Data curation: Ryan Jin-Young Kim, Ji-Man Park.

Funding acquisition: Ji-Man Park.

Investigation: Ryan Jin-Young Kim, Goran I. Benic, Ji-Man Park.

Validation: Ryan Jin-Young Kim, Goran I. Benic, Ji-Man Park.

Writing – original draft: Ryan Jin-Young Kim, Ji-Man Park.

Writing – review & editing: Ryan Jin-Young Kim, Goran I. Benic, Ji-Man Park.

References

1. Gjelvold B, Chrcanovic BR, Korduner EK, Collin-Bagewitz I, Kisch J. Intraoral digital impression technique compared to conventional impression technique. A randomized clinical trial. J Prosthodont. 2016;25(4):282-7. doi: 10.1111/jopr.12410 PMID: 26618259.
2. Mangano F, Gandolfi A, Luongo G, Logozzo S. Intraoral scanners in dentistry: a review of the current literature. BMC Oral Health. 2017;17(1):149. doi: 10.1186/s12903-017-0442-x PMID: 29233132.
3. Wismeijer D, Mans R, van Genuchten M, Reijers HA. Patients' preferences when comparing analogue implant impressions using a polyether impression material versus digital impressions (intraoral scan) of dental implants. Clin Oral Implants Res. 2014;25(10):1113-8. doi: 10.1111/clr.12234 PMID: 23941118.
4. Kim RJ, Park JM, Shim JS. Accuracy of 9 intraoral scanners for complete-arch image acquisition: A qualitative and quantitative evaluation. J Prosthet Dent. 2018;120(6):895-903 e1. doi: 10.1016/j.prosdent.2018.01.035 PMID: 30006228.
5. Rutkunas V, Geciauskaite A, Jegelevicius D, Vaitiekunas M. Accuracy of digital implant impressions with intraoral scanners. A systematic review. Eur J Oral Implantol. 2017;10 Suppl 1:101-20. PMID: 28944372.
6. Lee SJ, Betensky RA, Gianneschi GE, Gallucci GO. Accuracy of digital versus conventional implant impressions. Clin Oral Implants Res. 2015;26(6):715-9. doi: 10.1111/clr.12375 PMID: 24720423.
7. Katsoulis J, Takeichi T, Sol Gaviria A, Peter L, Katsoulis K. Misfit of implant prostheses and its impact on clinical outcomes. Definition, assessment and a systematic review of the literature. Eur J Oral Implantol. 2017;10 Suppl 1:121-38. PMID: 28944373.
8. Alikhasi M, Siadat H, Nasirpour A, Hasanzade M. Three-dimensional accuracy of digital impression versus conventional method: effect of implant angulation and connection Type. Int J Dent. 2018;2018:3761750. doi: 10.1155/2018/3761750 PMID: 29971107.
9. Menini M, Setti P, Pera F, Pera P, Pesce P. Accuracy of multi-unit implant impression: traditional techniques versus a digital procedure. Clin Oral Investig. 2018;22(3):1253-62. doi: 10.1007/s00784-017-2217-9 PMID: 28965251.
10. Papaspyridakos P, Gallucci GO, Chen CJ, Hanssen S, Naert I, Vandenberghe B. Digital versus conventional implant impressions for edentulous patients: accuracy outcomes. Clin Oral Implants Res. 2016;27(4):465-72. doi: 10.1111/clr.12567 PMID: 25682892.

11. Marghalani A, Weber HP, Finkelman M, Kudara Y, El Rafie K, Papaspyridakos P. Digital versus conventional implant impressions for partially edentulous arches: An evaluation of accuracy. J Prosthet Dent. 2018;119(4):574-9. doi: 10.1016/j.prosdent.2017.07.002 PMID: 28927923.
12. Basaki K, Alkumru H, De Souza G, Finer Y. Accuracy of digital vs conventional implant impression approach: A three-dimensional comparative in vitro analysis. Int J Oral Maxillofac Implants. 2017;32(4):792-9. doi: 10.11607/jomi.5431 PMID: 28618432.
13. Rhee YK, Huh YH, Cho LR, Park CJ. Comparison of intraoral scanning and conventional impression techniques using 3-dimensional superimposition. J Adv Prosthodont. 2015;7(6):460-7. doi: 10.4047/jap.2015.7.6.460 PMID: 26816576.
14. Ajioka H, Kihara H, Odaira C, Kobayashi T, Kondo H. Examination of the position accuracy of implant abutments reproduced by intra-oral optical impression. PLoS One. 2016;11(10):e0164048. doi: 10.1371/journal.pone.0164048 PMID: 27706225.
15. Alsharbaty MHM, Alikhasi M, Zarrati S, Shamshiri AR. A clinical comparative study of 3-dimensional accuracy between digital and conventional implant impression techniques. J Prosthodont. 2018. doi: 10.1111/jopr.12764 PMID: 29423969.
16. Lin WS, Harris BT, Elathamna EN, Abdel-Azim T, Morton D. Effect of implant divergence on the accuracy of definitive casts created from traditional and digital implant-level impressions: an in vitro comparative study. Int J Oral Maxillofac Implants. 2015;30(1):102-9. doi: 10.11607/jomi.3592 PMID: 25615919.
17. Tan MY, Yee SHX, Wong KM, Tan YH, Tan KBC. Comparison of three-dimensional accuracy of digital and conventional implant impressions: effect of interimplant distance in an edentulous arch. Int J Oral Maxillofac Implants. 2018. doi: 10.11607/jomi.6855 PMID: 30521661.
18. Vandeweghe S, Vervack V, Dierens M, De Bruyn H. Accuracy of digital impressions of multiple dental implants: an in vitro study. Clin Oral Implants Res. 2017;28(6):648-53. doi: 10.1111/clr.12853 PMID: 27150731.
19. van der Meer WJ, Andriessen FS, Wismeijer D, Ren Y. Application of intra-oral dental scanners in the digital workflow of implantology. PLoS One. 2012;7(8):e43312. doi: 10.1371/journal.pone.0043312 PMID: 22937030.
20. Flugge TV, Att W, Metzger MC, Nelson K. Precision of dental implant digitization using intraoral scanners. Int J Prosthodont. 2016;29(3):277-83. doi: 10.11607/ijp.4417 PMID: 27148990.

21. Imburgia M, Logozzo S, Hauschild U, Veronesi G, Mangano C, Mangano FG. Accuracy of four intraoral scanners in oral implantology: a comparative in vitro study. BMC Oral Health. 2017;17(1):92. doi: 10.1186/s12903-017-0383-4 PMID: 28577366.
22. Mangano FG, Veronesi G, Hauschild U, Mijiritsky E, Mangano C. Trueness and precision of four intraoral scanners in oral implantology: A comparative in vitro study. PLoS One. 2016;11(9):e0163107doi: 10.1371/journal.pone.0163107 PMID: 27684723.
23. Chew AA, Esguerra RJ, Teoh KH, Wong KM, Ng SD, Tan KB. Three-dimensional accuracy of digital implant impressions: Effects of different scanners and implant level. Int J Oral Maxillofac Implants. 2017;32(1):70-80. doi: 10.11607/jomi.4942 PMID: 27706264.
24. Gimenez B, Ozcan M, Martinez-Rus F, Pradies G. Accuracy of a digital impression system based on parallel confocal laser technology for implants with consideration of operator experience and implant angulation and depth. Int J Oral Maxillofac Implants. 2014;29(4):853-62. doi: 10.11607/jomi.3343 PMID: 25032765.
25. Gimenez B, Ozcan M, Martinez-Rus F, Pradies G. Accuracy of a digital impression system based on active triangulation technology with blue light for implants: Effect of clinically relevant parameters. Implant Dent. 2015;24(5):498-504. doi: 10.1097/ID.0000000000000283 PMID: 26057777.
26. Gimenez B, Pradies G, Martinez-Rus F, Ozcan M. Accuracy of two digital implant impression systems based on confocal microscopy with variations in customized software and clinical parameters. Int J Oral Maxillofac Implants. 2015;30(1):56-64. doi: 10.11607/jomi.3689 PMID: 25615916.
27. Park JM, Shim JS. Measuring the complete-arch distortion of an optical dental impression. J Vis Exp. 2019;(147). Epub 2019/06/18. doi: 10.3791/59261 PMID: 31205295.
28. Joda T, Lenherr P, Dedem P, Kovaltschuk I, Bragger U, Zitzmann NU. Time efficiency, difficulty, and operator's preference comparing digital and conventional implant impressions: a randomized controlled trial. Clin Oral Implants Res. 2017;28(10):1318-23. doi: 10.1111/clr.12982 PMID: 27596805.
29. Papaspyridakos P, Chen CJ, Gallucci GO, Doukoudakis A, Weber HP, Chronopoulos V. Accuracy of implant impressions for partially and completely edentulous patients: a systematic review. Int J Oral Maxillofac Implants. 2014;29(4):836-45. doi: 10.11607/jomi.3625 PMID: 25032763.

30. Andriessen FS, Rijkens DR, van der Meer WJ, Wismeijer DW. Applicability and accuracy of an intraoral scanner for scanning multiple implants in edentulous mandibles: a pilot study. J Prosthet Dent. 2014;111(3):186-94. doi: 10.1016/j.prosdent.2013.07.010 PMID: 24210732.

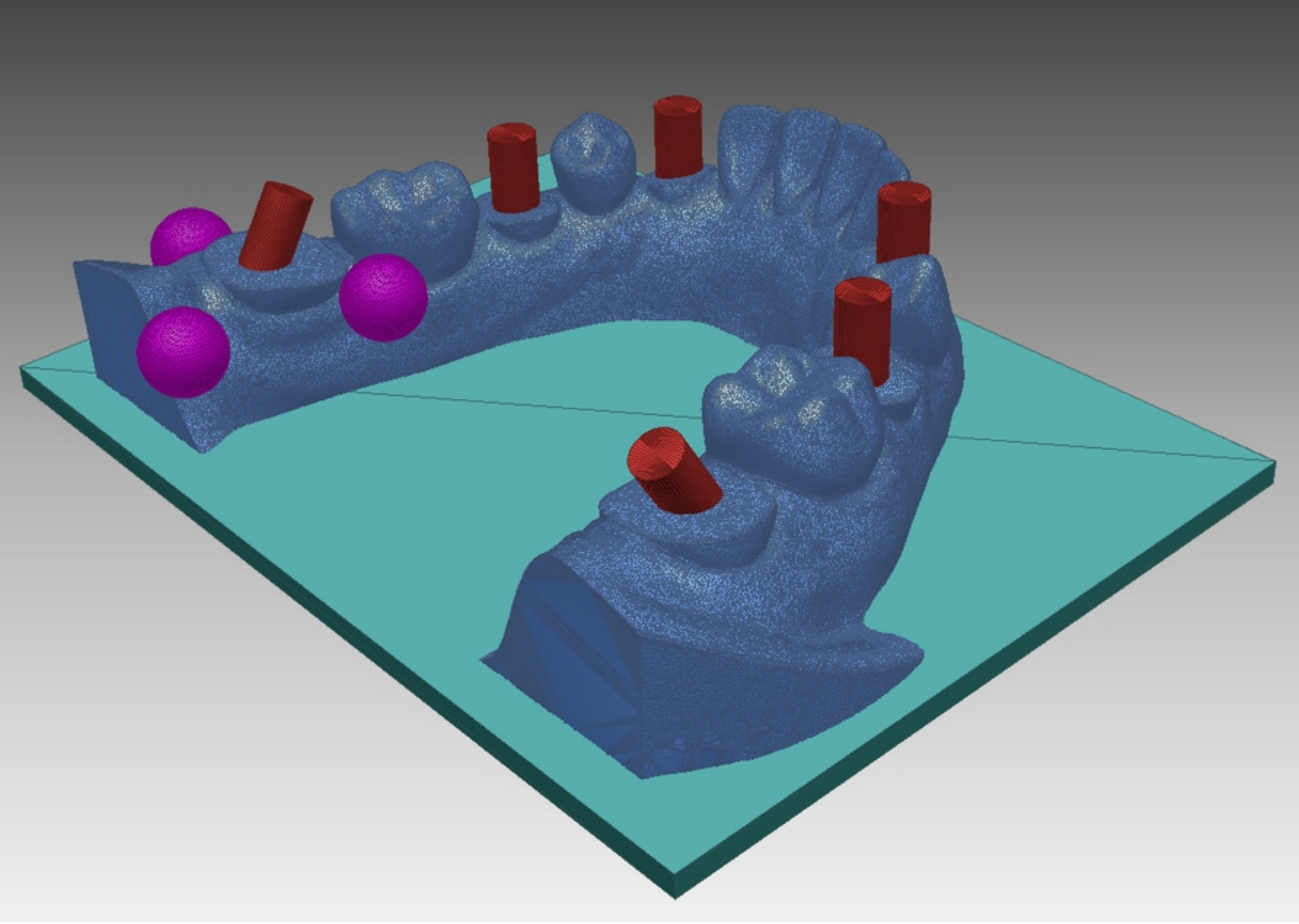

Figure 1A

Figure 1B

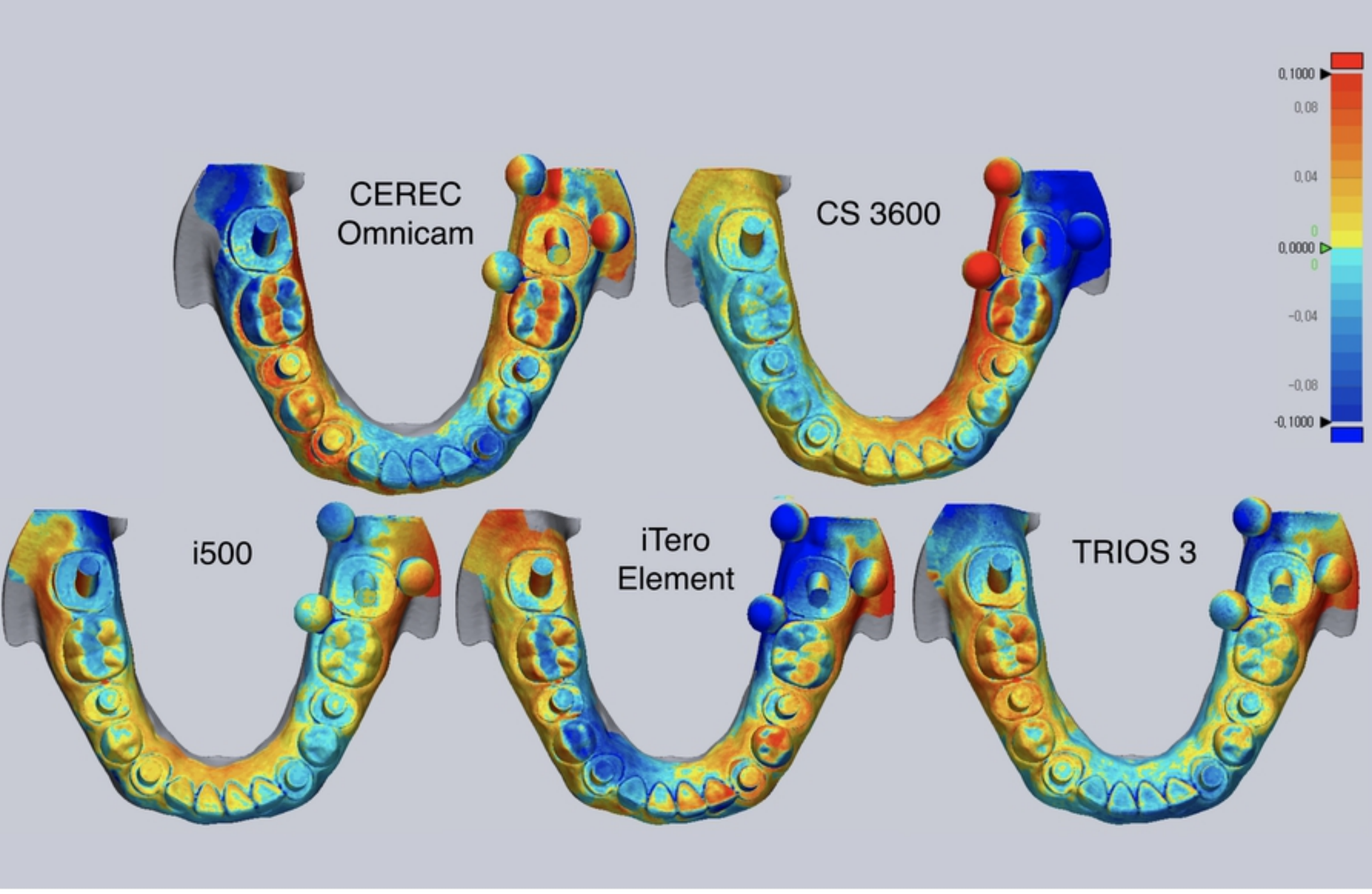
CEREC
Omnicam
CS 3600
i500
iTero
Element
TRIOS 3
0,1000
0,08
0,04
0
0,0000
0
-0,04
-0,08
-0,1000

Figure 3

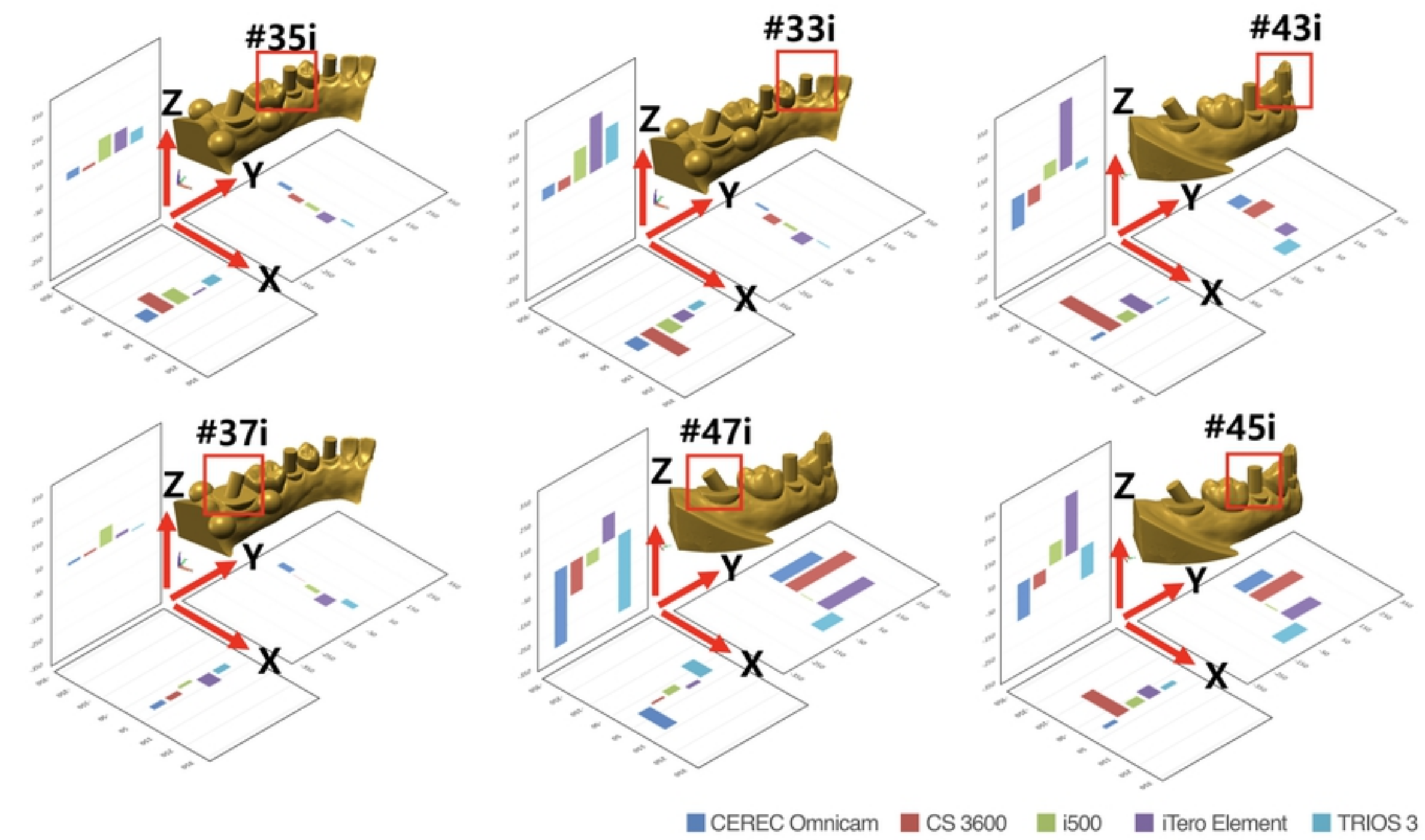
#35i
#33i
#43i
#37i
#47i
#45i
Z
Y
X
CEREC Omnicam
CS 3600
i500
iTero Element
TRIOS 3

Figure 2